

POLITECNICO DI TORINO  
Repository ISTITUZIONALE

A fully digital bridge towards the realization of the farad from the quantum Hall effect

*Original*

A fully digital bridge towards the realization of the farad from the quantum Hall effect / Marzano, Martina; Ortolano, Massimo; D'Elia, Vincenzo; Mueller, Andre; Callegaro, Luca. - In: METROLOGIA. - ISSN 0026-1394. - STAMPA. - 58:1(2021). [10.1088/1681-7575/abba86]

*Availability:*

This version is available at: 11583/2846664 since: 2020-09-24T20:56:23Z

*Publisher:*

Institute of Publishing

*Published*

DOI:10.1088/1681-7575/abba86

*Terms of use:*

This article is made available under terms and conditions as specified in the corresponding bibliographic description in the repository

*Publisher copyright*

IOP postprint/Author's Accepted Manuscript

"This is the accepted manuscript version of an article accepted for publication in METROLOGIA. IOP Publishing Ltd is not responsible for any errors or omissions in this version of the manuscript or any version derived from it. The Version of Record is available online at <http://dx.doi.org/10.1088/1681-7575/abba86>

(Article begins on next page)

# A fully digital bridge towards the realization of the farad from the quantum Hall effect

Martina Marzano<sup>1</sup>, Massimo Ortolano<sup>1,2</sup>, Vincenzo D'Elia<sup>1</sup>, André Müller<sup>3</sup> and Luca Callegaro<sup>1</sup>

<sup>1</sup> Istituto Nazionale di Ricerca Metrologica  
Strada delle Cacce, 91, 10135 Torino, Italy

<sup>2</sup> Politecnico di Torino

Corso Duca degli Abruzzi 24, 10129 Torino, Italy

<sup>3</sup> Physikalisch-Technische Bundesanstalt  
Bundesallee 100, 38116 Braunschweig, Germany

E-mail: m.marzano@inrim.it

**Abstract.** This paper presents the implementation of an electronic fully-digital impedance bridge optimized for  $RC$  comparisons with equal impedance magnitudes, together with an evaluation of the uncertainty. This bridge has been designed with the goal of realizing the farad directly from the quantum Hall effect with a bridge uncertainty component at the  $10^{-7}$  level. Thanks to its simple design, ease of operation and affordability, this bridge is suitable to be industrially manufactured. Together with the increasing availability of graphene quantum Hall resistance standards, this can provide an affordable quantum realization of the unit farad for metrology institutes and calibration centres.

In this paper we present the uncertainty budget of an example measurement and the results of the validation of the bridge against a suitably modified version of the traceability chain of the Italian national standard of capacitance. The combined uncertainty of the bridge resulted from repeated measurements (overall measurement time of about 200 min) is  $9.2 \times 10^{-8}$ , suitable for the primary realization of the unit of capacitance from a quantized Hall resistance standard. The crosstalk among the channels of the electrical generator is the most significant uncertainty component, possibly reducible with internal shielding and filtering of the electronic generator.

PACS numbers: 06.20.fb, 06.30.Ka

Submitted to: *Metrologia*

## 1. Introduction

In the International System of Units (SI), the units of electrical impedance ohm, henry and farad are linked by the relations  $1\Omega = 1\text{Hs}^{-1} = 1\text{F}^{-1}\text{s}$ . Since the 2018 revision of the SI,

The farad F can be realized [...] by comparing the impedance of a known resistance obtained using the quantum Hall effect and the value of the von Klitzing constant [...], including a quantized Hall resistance itself, to the impedance of an unknown capacitance using, for example, a quadrature bridge; [...] [1, appendix 2]

The *quadrature bridge* mentioned in the SI brochure is a double product impedance bridge [2, 3], which compares two resistors  $R_1$  and  $R_2$ , and two capacitors  $C_1$  and  $C_2$ , at a properly chosen fixed angular frequency  $\omega$ . The standard implementation of the quadrature bridge principle [4–8] results in a very complex electrical network with many electromagnetic components, including several multi-decade inductive voltage dividers. These variable dividers must be skilfully operated in order to achieve both the two main balances and, simultaneously, several auxiliary ones. The latter are in fact required to match the proper impedance definition of each of the four standards being compared. Automating the quadrature bridge, although possible, is cumbersome [9, 10]. Digitally-assisted implementations [11, 12] can reduce the network complexity of the quadrature bridge to some extent, and allow a partial automation. A quadrature bridge calibrates the product  $C_1C_2$ ; an additional measurement with a ratio bridge is required to determine the individual values of  $C_1$  and  $C_2$ .

The quoted SI brochure entails that  $R_1$  and  $R_2$  are either resistance standards having an AC value traceable to a quantized Hall resistance (QHR) standard, or that they are QHR standards themselves, measured in the AC regime (ACQHR standards). In the first case [12–14], special resistors having a calculable frequency dependence [15, 16] are calibrated in DC versus the QHR, and their values are numerically corrected. In the second case [6, 17], the effect of unwanted frequency dependencies caused by parasitic effects in the Hall device must be carefully considered [18, 19]. To date, only one laboratory worldwide operates a permanent quadrature bridge

with two quantum Hall effect devices in a single cryostat [17], a massive and complex experiment filling an entire laboratory.

Fully-digital bridges [20–25] can compare a single resistor  $R$  and a single capacitor  $C$ . The fully-digital approach allows the design and implementation of much simpler bridges suitable to be industrially manufactured. Together with the increasing availability of quantum Hall graphene devices, which allow the realization of QHR standards in simpler experimental environments [26], the fully-digital approach underpins an affordable quantum realization of the unit farad by metrology institutes and calibration centres [27].

In the following, we present an electronic<sup>‡</sup> fully-digital bridge suitable for the realization of the farad<sup>§</sup>. The bridge calibrates a capacitance standard of nominal value 8 nF versus a resistor  $R$  of nominal value  $R_H = R_K/2 \approx 12\,906\,\Omega$  at the frequency<sup>||</sup>  $f \approx 1541\text{ Hz}$ .

The bridge network is very simple and is based on a multi-channel polyphase electronic digital waveform generator [33]. The bridge balance is semi-automated, and the duration of an individual measurement is around 15 min. The transfer relative expanded uncertainty is about  $3 \times 10^{-7}$  in a single measurement (15 min) and down to  $2 \times 10^{-7}$  in about 5 measurements (75 min).

This work reports the principle of operation of the bridge (section 2), its implementation (section 3), a thorough analysis of the uncertainty sources (section 4), and a validation of the bridge performance, by comparison with the traceability chain of the Italian national standard of capacitance [12] (section 5).

## 2. Principle of operation

The *four-terminal-pair voltage-ratio fully-digital* impedance bridge described herewith is based on the prin-

<sup>‡</sup> Here, the adjective *electronic* refers to the fact that the signal generator is based on integrated electronics, in contrast with fully-digital bridges based on Josephson arbitrary waveform synthesizers [28–31].

<sup>§</sup> This paper is focussed on the bridge description and on its measurement capabilities; its integration with a quantum Hall effect system is under development and will be reported in a future work.

<sup>||</sup> The nominal values for  $C$  and  $f$  are chosen to fulfil the relationship  $2\pi fRC \approx 1$ . The integer value  $C = 8\text{ nF} = 2^3\text{ nF}$  allows efficient scaling to the decadal values of interest for dissemination; the frequency  $f \approx 1541\text{ Hz}$  is close to  $1592\text{ Hz} \approx 10\text{ kHz}/(2\pi)$ , a *de facto* standard frequency for capacitance dissemination and intercomparisons [32].

ciple schematic of figure 1, where the coaxial shield and terminal pairs, and a number of auxiliary components have been omitted for simplicity (the complete schematic is reported in section 3).

The driving voltages and currents  $E_1$ ,  $E_2$ ,  $E_0$ ,  $E_L$ ,  $I_1$  and  $I_2$  are synthesized by a polyphase digital sinusoidal waveform generator operating at frequency  $f$  and can be individually adjusted in magnitude and phase¶. Each voltage or current corresponds to an output channel of the generator.  $E_1$  and  $E_2$  are the bridge main voltages;  $E_L$ ,  $I_1$  and  $I_2$  are auxiliary voltage and currents needed to realize the impedance definition; and  $E_0$  is an auxiliary injection voltage which, together with the injection impedance  $Z_0$ , allows to fine-tune the bridge balance.

The impedances under comparison are  $Z_1$ , with terminals HC1, HP1, LC1 and LP1, and  $Z_2$ , with terminals HC2, HP2, LC2 and LP2. In this specific application,  $Z_1$  is the reference impedance that can be either an ACQHR standard with resistance  $R_H$ , connected with a multiple-connection scheme (see section 6), or a calibrated standard resistor with nominal resistance  $R_H$ , such that  $Z_1 \approx R_H$ ;  $Z_2$  is a capacitor with capacitance  $C$ , such that  $Z_2 \approx 1/(j2\pi fC)$ ; and  $f$  is chosen so that  $2\pi fR_H C \approx 1$  (that is,  $Z_1/Z_2 \approx j$ ).

The bridge is balanced when  $V_{LP1} = V_{LP2} = 0$  and  $I_{HP1} = I_{HP2} = 0$ , where the voltages  $V_{LP1}$  and  $V_{LP2}$  are measured at the impedance terminals LP1 and LP2, and the currents  $I_{HP1}$  and  $I_{HP2}$  are measured at the detection terminals DHP1 and DHP2 through the current transformers CT<sub>1</sub> and CT<sub>2</sub>. The balance can be checked by cycling the synchronous detector D, referenced at the frequency  $f$ , through the detection terminals LP1, LP2, DHP1 and DHP2, and can be attained by adjusting  $E_2$  (or  $E_1$ ),  $E_0$ ,  $E_L$ ,  $I_1$  and  $I_2$  (the details of the balance procedure are discussed in section 3).

When the bridge is balanced, the impedance ratio  $Z_1/Z_2$  is directly compared with the voltage ratio  $E_1/E_2$ , and the following balance equation holds:

$$W = \frac{Z_1}{Z_2} = -\frac{E_1}{E_2} \left( 1 + \frac{E_0/Z_0}{E_1/Z_1} \right). \quad (1)$$

Alternatively, by considering the admittances  $Y_1 = 1/Z_1$ ,  $Y_2 = 1/Z_2$  and  $Y_0 = 1/Z_0$ ,

$$W = \frac{Y_2}{Y_1} = -\frac{E_1}{E_2} \left( 1 + \frac{E_0 Y_0}{E_1 Y_1} \right). \quad (2)$$

As can be seen from the above equations, by choosing  $|Z_0| \gg |Z_1|$ , the voltage  $E_0$  can be used to fine-tune the bridge balance around the ratio  $-E_1/E_2$ . This

¶ In the following, quantity symbols represent complex phasors associated to real voltage and current signals, or complex impedances.

is instrumental to achieve the highest measurement accuracy, as described below.

The voltage phasors  $E_1$  and  $E_2$  can be computed from the samples used to synthesize the two waveforms. We take the readings  $E_1^{\text{read}}$  and  $E_2^{\text{read}}$  from the fundamental components at frequency  $f$  of the Fourier series representing the waveform samples. Due to the generator non-idealities, the actual voltages will differ from the readings and we can write  $E_k = [1 + g_k(E_k^{\text{read}})]E_k^{\text{read}}$ ,  $k = 1, 2$ , with  $g_k(E_k^{\text{read}})$  representing a possibly voltage-dependent complex gain error (for magnitude and phase errors), thus considering a possible generator non-linearity. This is actually the main source of error in fully-digital bridges [23, 34].

The error described above can be perfectly cancelled by performing two measurements: one with the impedances connected as in figure 1 (*forward* configuration) and one with the two impedances exchanged (*reverse* configuration), and by imposing that the samples used to generate  $E_1$  and  $E_2$  are *exactly* the same in the two configurations, at most shifted in time, as shown on the left of figure 1 (how this condition can be imposed is described in section 3). This is feasible because with the conditions introduced at the beginning of this section, the magnitude of the impedance ratio is about 1 in both the forward and reverse configurations,  $|Z_2/Z_1| \approx |Z_1/Z_2| \approx 1$ , and its phase changes by about  $180^\circ$  because  $\arg(Z_2/Z_1) = -\arg(Z_1/Z_2) \approx 90^\circ$ . Therefore, to balance the reverse configuration, we just need to change the sign of all the samples of either  $E_1$  or  $E_2$  (equivalent to a  $180^\circ$  shift), and re-adjust the injection voltage  $E_0$ .

For the forward (F subscript) and reverse (R subscript) configurations, the balance equations are

$$W = W_F = -\frac{E_{1F}}{E_{2F}} \left( 1 + \frac{E_{0F}Y_0}{E_{1F}Y_1} \right), \quad (3)$$

$$W = W_R = -\frac{E_{2R}}{E_{1R}} \left( 1 + \frac{E_{0R}Y_0}{E_{2R}Y_1} \right), \quad (4)$$

from which

$$W = \sqrt{W_F W_R}, \quad (5)$$

where the complex square root in (5) should be determined with a positive imaginary part because  $W \approx j$ .

According to the foregoing argument,  $E_{1R}/E_{2R} = -E_{1F}/E_{2F}$ , *exactly*, by construction of the waveform samples, such that, from (3)–(5),

$$W = j \sqrt{\left( 1 + \frac{E_{0F}Y_0}{E_{1F}Y_1} \right) \left( 1 + \frac{E_{0R}Y_0}{E_{2R}Y_1} \right)}, \quad (6)$$

thus cancelling any major error due to  $g_k(E_k^{\text{read}})$  (minor errors are discussed in section 4).

From  $W$  and the reference impedance  $Z_1$ , the capacitance  $C$  can be finally determined as

$$C = \frac{1}{2\pi f} \operatorname{Im} \frac{W}{Z_1} = \frac{1}{2\pi f} \operatorname{Im}(W Y_1), \quad (7)$$

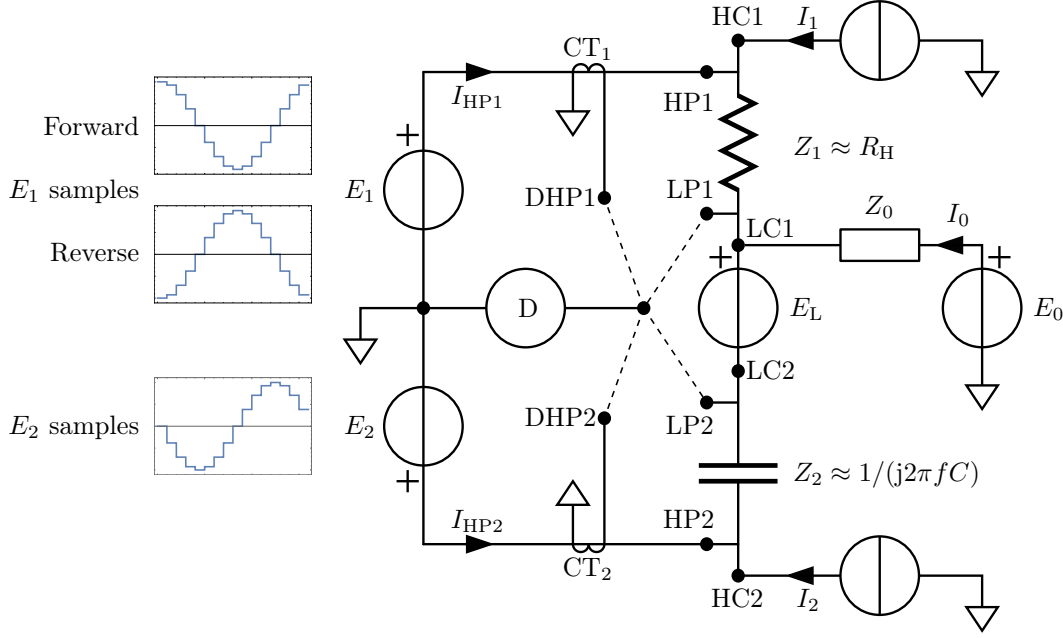


**Figure 1.** Simplified principle schematic of the bridge:  $Z_1 \approx R_H$  and  $Z_2 \approx 1/(j2\pi fC)$  are the impedances under comparison;  $f$  is the bridge operating frequency, chosen so that  $2\pi f R_H C \approx 1$ ;  $E_1$  and  $E_2$  are the main bridge voltages;  $I_1$  and  $I_2$  are the current sources balancing  $I_{HP1}$  and  $I_{HP2}$ ;  $E_L$  is the voltage source balancing the difference  $V_{LP1} - V_{LP2}$ ;  $CT1$  and  $CT2$  are current transformers measuring the currents  $I_{HP1}$  and  $I_{HP2}$ , respectively; the voltage source  $E_0$  and the impedance  $Z_0$  constitute an auxiliary injection arm to fine-tune the bridge balance; and  $D$  is a synchronous detector that can be connected, in turn, to the detection terminals  $LP1$ ,  $LP2$ ,  $DHP1$  and  $DHP2$ . The diagrams on the left represent example waveform samples: the samples of  $E_1$  are changed in sign between the forward and reverse configurations; the samples of  $E_2$  are instead kept fixed.

where  $\text{Im}$  denotes the imaginary part of its argument.

### 3. Bridge implementation

Figures 2 and 3 show the coaxial schematic and a photograph of the bridge.

This section describes only the implementation of the bridge network; the impedances  $Z_1$  and  $Z_2$  employed in the validation are described in section 5.

At the core of the bridge there is the adjustable polyphase digital sinusoidal waveform generator described in [35]<sup>+</sup>. This digital signal source is based on 18 bit digital-to-analogue converters (DACs) with adjustable range (1 V, 2.5 V, 5 V and 10 V) and isolated precision filter/buffer output stages [37]. The relative amplitude and phase stability of the source are about  $10^{-7}/\text{h}$ . A National Instruments NI-DAQ 6541 board generates the digital codes of the waveform samples, which are then transmitted to the source. The waveform is composed of a fixed integer number of samples per period\* and the frequency is adjusted through the

sample rate and the number of samples. This yields the possibility to control the output samples and obtain a simple and computable output spectrum. A channel reading is then obtained from the latter. The clock of the digital source, which defines the sample rate, is locked to a 10 MHz signal from the Italian national time scale.

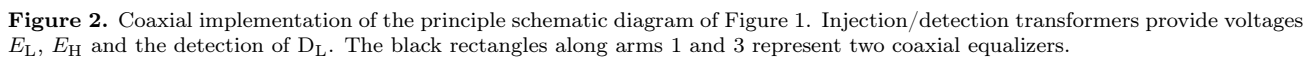
The digital source provides seven independent output channels, necessary for the complete implementation of the bridge. Two channels generate the voltages  $E_1$  and  $E_2$ , which provide the voltage ratio reference against which the impedance ratio is compared. The  $R_{S1} = R_{S2} = 10 \Omega$  resistors (Vishay S102 series), in series to  $E_1$  and  $E_2$ , isolate the channel outputs from the capacitive load, avoiding possible self-oscillations of the output buffers.

Three channels generate the voltages  $E_3$ ,  $E_4$  and  $E_L$  which drive the auxiliary circuits realizing the four terminal-pair impedance definition. The currents  $I_1$  and  $I_2$  are generated by  $E_3$  and  $E_4$  through the  $R_{S3} = R_{S4} = 100 \Omega$  resistors (Vishay S102 series). Two dummy loads  $C_L \approx C$  and  $R_L \approx R_H$  are added at the HC ports of the impedances to symmetrize the source loading in both forward and reverse configurations.

One channel generates the voltage  $E_L$  through a with phase accumulation [38].

<sup>+</sup> The generator was developed by Janusz Kaczmarek and Ryszard Rybski, University of Zielona Góra (UZG), Poland, in the framework of the European project EMRP SIB53 AIM QuTE: Automated impedance metrology extending the quantum toolbox for electricity [36].

\* Unlike what happens in a direct-digital synthesizer (DDS)



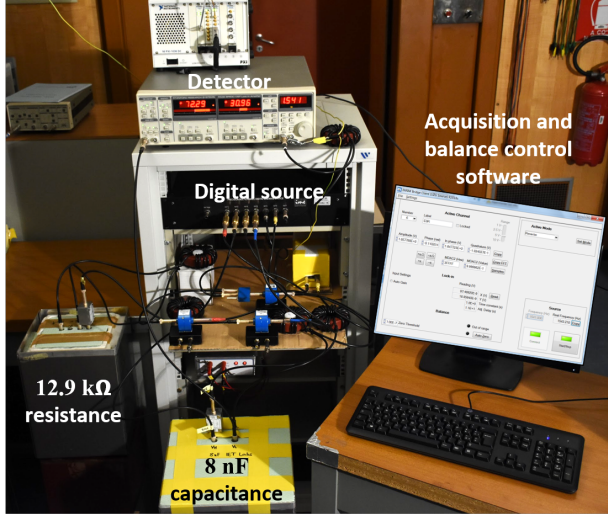


**Figure 3.** Picture of the experimental set-up.

200 : 1 feedthrough injection voltage transformer. One channel generates the voltage  $E_0$  which provides the auxiliary injection through the  $C_0 = 1\text{ pF}$  capacitor, which corresponds to  $Z_0$  in figure 1. One further channel generates the reference signal for the phase-sensitive detector.

The phase-sensitive detector is a Stanford Research SR830 lock-in amplifier and is used to detect the bridge balance on the fundamental component of the signal.

The detector is manually switched across the positions  $V_{DHP1}$  and  $V_{DHP2}$ , measuring the currents  $I_{HP1}$  and  $I_{HP2}$  through the 1 : 200 feedthrough transformers  $CT_1$  and  $CT_2$ , and the positions  $V_{LP1}$  and  $V_{LP2}$ .

Both the digital source and the detector are controlled by a software purposely coded in the National Instruments LabWindows/CVI environment and based on the balancing algorithm presented in [39]. The bridge balance procedure is thus semi-automated and a single complete measurement (forward/reverse) requires about 15 min. According to what was introduced in section 2, when switching between the forward and reverse configurations, we can change the phase of  $E_1$  by  $180^\circ$  and keep  $E_2$  fixed. The digital source employed in this implementation allows to read the generated samples verifying that they are exactly matched with a  $180^\circ$  phase shift.

Before beginning a series of measurements, it is convenient to preset the main voltages  $E_1$  and  $E_2$  to minimize the auxiliary injection  $E_0$ . Starting from the set-up shown in figure 2, the preliminary procedure can be done in the following way:

P1. Set  $E_0$  to 0V, and  $E_1$  to the operating value of interest.

- P2. Short circuit both  $V_{LP1}$  and  $V_{LP2}$ .
- P3. Adjust  $E_3$  to null the detector connected to  $V_{DHP1}$ .
- P4. Adjust  $E_4$  to null the detector connected to  $V_{DHP2}$ .
- P5. Remove the short circuit at  $V_{LP1}$ .
- P6. Adjust  $E_5$  to null the detector connected to  $V_{LP1}$  (this actually nulls the differential voltage  $V_{LP1} - V_{LP2}$ ).
- P7. Remove the remaining short circuit at  $V_{LP2}$ .
- P8. Adjust  $E_2$  to null the detector connected to  $V_{LP1}$ .
- P9. Adjust  $E_4$  to null the detector connected to  $V_{DHP2}$ .
- P10. Repeat steps P8 and P9 until the detector is nulled simultaneously within the chosen thresholds for both detection ports.
- P11. Record the voltage reading  $E_{2F}^{\text{read}}$  for the forward configuration.
- P12. Change set-up from the forward configuration to the reverse one by swapping the cables between  $E_1 \leftrightarrow E_2$  and  $E_3 \leftrightarrow E_4$ , and by shifting the phase of  $E_1$  by  $180^\circ$ .
- P13. Repeat steps P1 through P10 and record the voltage reading  $E_{2R}^{\text{read}}$  for the reverse configuration.
- P14. Set  $E_2$  in both configurations to the geometric mean  $E_2 = \sqrt{E_{2F}^{\text{read}} E_{2R}^{\text{read}}}$ .

The measurement procedure is then as follows:

- M1. In the forward configuration, execute the steps P2 through P7 of the preliminary procedure and finally adjust  $E_0$  to null the detector connected to  $V_{LP1}$ . Record the readings  $E_{0F}^{\text{read}}$ ,  $E_{1F}^{\text{read}}$  and  $E_{2F}^{\text{read}}$ .
- M2. In the reverse configuration, execute the steps P2 through P7 of the preliminary procedure and finally adjust  $E_0$  to null the detector connected to  $V_{LP1}$ . Record the readings  $E_{0R}^{\text{read}}$ ,  $E_{1R}^{\text{read}}$  and  $E_{2R}^{\text{read}}$ .
- M3. Calculate  $W$  from (19), section 4.5.
- M4. The capacitance  $C$  is determined, from  $W$  and the impedance  $Z_1$ , as in (7).

We note the following: i) even though the bridge balance procedure can be completely automated with an external switch, we preferred the semi-automated approach to avoid the risk of worsening the crosstalk between the source channels (see section 4.2); and ii) the steps P5 and P6 of the preliminary procedure can be substituted with a measurement with the detector set in the differential input configuration.

#### 4. Uncertainty sources and budget

This section presents an evaluation of the uncertainty for the ratio  $W = Z_1/Z_2$  as defined by (5). The

uncertainty sources are first described separately and then the relevant ones are combined in a measurement model which is used in reporting the uncertainty budget (for a review on the error sources in digital impedance bridges see also [34]).

In the following, according to the notation introduced in section 2, the subscripts “F” and “R” designate quantity values obtained in the forward and reverse configurations, respectively; the superscript “read” designates quantity values read off the generator settings, as described in section 1. From (3)–(5) we also define

$$W_F^{\text{read}} = -\frac{E_{1F}^{\text{read}}}{E_{2F}^{\text{read}}} \left( 1 + \frac{E_{0F}^{\text{read}} Y_0}{E_{1F}^{\text{read}} Y_1} \right), \quad (8)$$

$$W_R^{\text{read}} = -\frac{E_{2R}^{\text{read}}}{E_{1R}^{\text{read}}} \left( 1 + \frac{E_{0R}^{\text{read}} Y_0}{E_{2R}^{\text{read}} Y_1} \right) \quad (9)$$

and

$$W^{\text{read}} = \sqrt{W_F^{\text{read}} W_R^{\text{read}}}. \quad (10)$$

#### 4.1. Type A uncertainty

In this experiment, the type A uncertainty mainly depends on the noise at the detection ports LP1, LP2, DHP1 and DHP2, on the mutual impedance  $Z_m$  of the current transformers CT1 and CT2, on the detector time constants and thresholds chosen to stop the bridge balancing at the various detection ports, and on the instabilities of the source and the standards.

The contribution of the low balance to the type A uncertainty component of  $W$ , for a single measurement, should be expected of the order of  $|\delta V_L/E_{1,2}|$ ,  $\delta V_L$  being the spread of the residual voltages at LP1 and LP2. The contribution of the high balance should be expected of the order of  $|R_{s1,s2} \delta V_H/(Z_m E_{1,2})|$ ,  $\delta V_H$  being the spread of the residual voltages at DHP1 and DHP2 (see [34] for a more detailed analysis).

For the current setup we set the thresholds for the balances at LP1 and LP2 to 30 nV (1 s detector time constant) and the thresholds for the balances at DHP1 and DHP2 to 200 nV (300 ms detector time constant). With these settings, taking into account that  $|Z_m| \approx 240 \Omega$ , the projected type A uncertainty component is about  $10^{-7}$  for a single measurement.

#### 4.2. Crosstalk

Crosstalk is the phenomenon by which the voltage at one channel of the polyphase generator is coupled to that of another channel. Considering just the channels that may induce significant variations when switching between the forward and reverse configurations, and that  $E_3 \approx E_1$  and  $E_4 \approx E_2$ , we can therefore write

$$E_1 = E_1^{\text{read}} + E_{10} + a_{12} E_2^{\text{read}} + a_{10} E_0^{\text{read}}, \quad (11)$$

$$E_2 = E_2^{\text{read}} + E_{20} + a_{21} E_1^{\text{read}} + a_{20} E_0^{\text{read}}. \quad (12)$$

In the above equations,  $E_{10}$  and  $E_{20}$  represent possible residual voltages at the source outputs, independent of  $E_0^{\text{read}}$ ,  $E_1^{\text{read}}$  and  $E_2^{\text{read}}$ , and which can be due to the crosstalk from  $E_{\text{ref}}$  or a clock feedthrough; and  $a_{ij}$  is the (complex) coupling coefficient from channel  $j$  to channel  $i$ .

Due to crosstalk, the equality  $E_{1R}/E_{2R} = -E_{1F}/E_{2F}$ , obtained in section 1 from the construction of the samples, no longer holds exactly. As a consequence, an error arises. By combining (11) and (12) with (3)–(5), and simplifying, we obtain at first order in the coupling coefficients

$$W = W^{\text{read}} - \Delta W^{\text{CT}} \quad (13)$$

with the error  $\Delta W^{\text{CT}}$  given by

$$\begin{aligned} \frac{\Delta W^{\text{CT}}}{W^{\text{read}}} \approx & -\frac{1}{2} \left[ E_{10} \left( \frac{1}{E_{1F}^{\text{read}}} - \frac{1}{E_{1R}^{\text{read}}} \right) \right. \\ & - E_{20} \left( \frac{1}{E_{2F}^{\text{read}}} - \frac{1}{E_{2R}^{\text{read}}} \right) + a_{12} \left( \frac{E_{2F}^{\text{read}}}{E_{1F}^{\text{read}}} - \frac{E_{2R}^{\text{read}}}{E_{1R}^{\text{read}}} \right) \\ & - a_{21} \left( \frac{E_{1F}^{\text{read}}}{E_{2F}^{\text{read}}} - \frac{E_{1R}^{\text{read}}}{E_{2R}^{\text{read}}} \right) + a_{10} \left( \frac{E_{0F}^{\text{read}}}{E_{1F}^{\text{read}}} - \frac{E_{0R}^{\text{read}}}{E_{1R}^{\text{read}}} \right) \\ & \left. - a_{20} \left( \frac{E_{0F}^{\text{read}}}{E_{2F}^{\text{read}}} - \frac{E_{0R}^{\text{read}}}{E_{2R}^{\text{read}}} \right) \right]. \quad (14) \end{aligned}$$

The measured average magnitudes of  $E_{10}$  and  $E_{20}$  are of the order 30 nV, with a high phase uncertainty. For a reasonably conservative evaluation of the uncertainty, for  $E_{10}$  and  $E_{20}$ , we assumed uncorrelated real and imaginary parts centred around 0 with a standard uncertainty of 30 nV for each part, corresponding to a square coverage region. The measured magnitudes of the coupling coefficients between the different channels of the polyphase generator are less than  $2 \times 10^{-8}$ , with a high phase uncertainty. For these coefficients, we assumed uncorrelated real and imaginary parts centred around 0 with a standard uncertainty of  $2 \times 10^{-8}$  for each part.

#### 4.3. Injection uncertainty

The injection terms in (3) and (4) depend on the voltage ratios  $E_{0F}/E_{1F}$ ,  $E_{0R}/E_{2R}$  and on the admittances  $Y_0$  and  $Y_1$ . The voltage ratios can be written as

$$\frac{E_{0F}}{E_{1F}} = (1 + g_{01}) \frac{E_{0F}^{\text{read}}}{E_{1F}^{\text{read}}} \quad (15)$$

and

$$\frac{E_{0R}}{E_{2R}} = (1 + g_{02}) \frac{E_{0R}^{\text{read}}}{E_{2R}^{\text{read}}} \quad (16)$$

where the complex error terms  $g_{01}$  and  $g_{02}$  account for the generator non-linearity as described in section 1.

A characterization of the source yielded for  $1 + g_{01}$  and  $1 + g_{02}$  a magnitude uncertainty of about  $10^{-4}$  and an angle uncertainty of about  $10^{-4}$  rad. The

uncertainty contributions of  $Y_0$  and  $Y_1$  are typically negligible.

#### 4.4. Source loading

When the bridge is balanced, the currents crossing CT1 and CT2 are approximately zero, but  $E_1$  and  $E_2$  are still loaded by the stray capacitances  $C_{H1}$  and  $C_{H2}$  of the cables connecting the channels to the current transformers.

When reversing the channels at the source ports, as is done in this experiment, this causes an error such that [23, 34]

$$W \approx W^{\text{read}} \left[ 1 - \frac{1}{2}(R_{s1} + R_{s2})(Y_{H1} - Y_{H2}) \right] \quad (17)$$

$$\approx W^{\text{read}} [1 - j\pi f(R_{s1} + R_{s2})(C_{H1} - C_{H2})], \quad (18)$$

where  $Y_{H1}$  and  $Y_{H2}$  are the admittances of  $C_{H1}$  and  $C_{H2}$ , respectively. If the bridge construction is symmetric, the difference  $C_{H1} - C_{H2}$  is small. Since  $W^{\text{read}} \approx j$ , the expression in the brackets changes at first order only the real part of  $W^{\text{read}}$  and not its imaginary part. Therefore, from (7), the resulting error on  $C$  is negligible at the target uncertainty level of this experiment and will not be considered in the measurement model of the next section.

#### 4.5. Measurement model and uncertainty budget

By combining the above results with (6), we obtain the measurement model

$$W = j \sqrt{\left[ 1 + (1 + g_{01}) \frac{E_{0F}^{\text{read}} Y_0}{E_{1F}^{\text{read}} Y_1} \right] \left[ 1 + (1 + g_{02}) \frac{E_{0R}^{\text{read}} Y_0}{E_{2R}^{\text{read}} Y_1} \right] - \Delta W^{\text{CT}}}. \quad (19)$$

Table 1 reports the uncertainty budget of an example measurement for the quantity  $\Delta = \text{Im } W - 1$  (because  $W \approx j$ ). All the uncertainties are standard uncertainties ( $k = 1$ ). The measurement was performed on 20 February 2020 and it is also discussed in section 5.1. The driving rms voltages  $|E_{1,2}| \approx 0.25$  V are chosen so that the driving current  $I \approx 20$   $\mu$ A flowing in the standards is suitable for the QHR. We performed the propagation of uncertainty according to [40] with the help of *Metas.UncLib* [41].

The measurement consisted in  $n = 13$  repetitions of forward and reverse measurements, for an overall measurement time of about 200 min and a type A uncertainty component of  $2.2 \times 10^{-8}$ , in reasonable agreement with the value obtainable from the projection of section 4.1 ( $\approx 10^{-7}/\sqrt{13}$ ). The most significant uncertainty component is that associated to  $\Delta W^{\text{CT}}$ , which was evaluated from (14) and the measurements of the coupling coefficients.

The combined uncertainty is  $u_c(\Delta) \approx 9.2 \times 10^{-8}$ , which is competitive for the primary realization of the

**Table 1.** Example uncertainty budget for  $\Delta = \text{Im } W - 1$ . All the uncertainties are standard uncertainties ( $k = 1$ ).

$i$	Quantity	Type	$u_i(\Delta) \times 10^6$
1	Bridge reading ( $n = 13$ )	A	0.022
2	Crosstalk ( $\Delta W^{\text{CT}}$ )	B	0.089
5	Injection	B	0.01
RSS			0.092

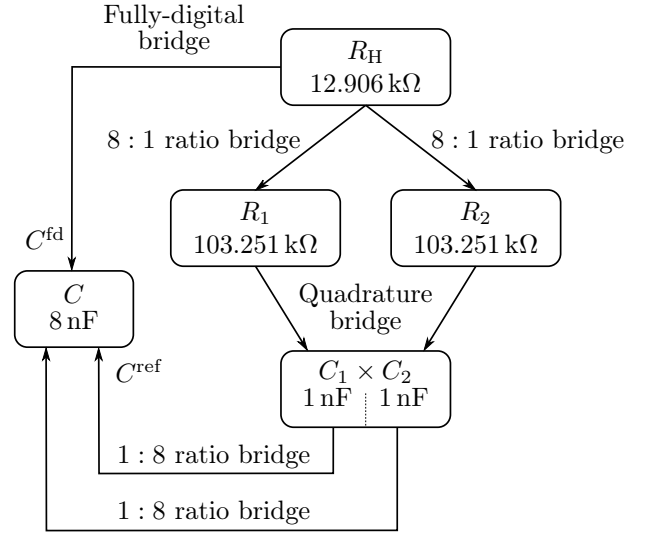


**Figure 4.** Diagram of the procedure adopted to compare the calibration of the 8 nF capacitance standard performed with the four-terminal-pair fully-digital bridge and that performed with the traceability chain of the Italian national standard of capacitance.

unit of capacitance. Since the type A uncertainty is much smaller than the type B, 5 measurements are enough to reach a combined uncertainty of  $2 \times 10^{-7}$ .

## 5. Validation

The validation of the bridge performance was obtained by comparing the 8 nF capacitor calibration performed with the four-terminal-pair fully-digital bridge with that performed with the traceability chain of the Italian national standard of capacitance [12]. The latter is typically employed to calibrate a 1 nF capacitance standard against a calibrated 12 906  $\Omega$  quadrifilar resistance standard, but it is here adapted to calibrate the 8 nF capacitance standard.

Figure 4 shows the measurement chain adopted in the validation process.

On one side of the chain, two resistance standards  $R_1$  and  $R_2$  of nominal value  $R_{1,2} \approx 8R_H \approx 103.251 \text{ k}\Omega$  are calibrated with a 8 : 1 transformer-ratio resistance bridge against a resistance standard of nominal value  $R_H = R_K/2 \approx 12 906 \Omega$ . These resistance standards

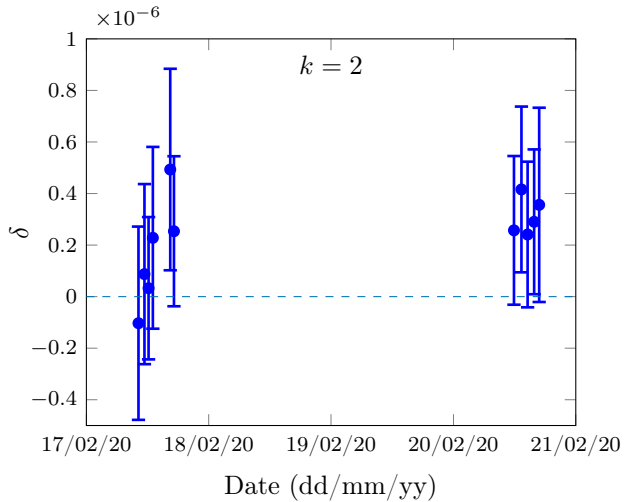


**Figure 5.** Comparison between the calibrations of an 8 nF capacitance standard performed with the four-terminal-pair fully-digital bridge described in the paper and with the Italian capacitance traceability chain, suitably modified. The plot represents the quantity  $\delta = (C^{\text{fd}} - C^{\text{ref}})/C^{\text{ref}}$ .

are then employed in a transformer-ratio quadrature bridge to calibrate the product  $C_1 C_2$  of two 1 nF capacitance standards. By means of a double calibration of the 8 nF capacitance standard against  $C_1$  and  $C_2$  with a 1 : 8 transformer-ratio bridge,  $C^{\text{ref}}$  is then obtained from the product  $C_1 C_2$ .

On the other side, the calibration  $C^{\text{fd}}$  of the 8 nF is performed with the four-terminal-pair fully-digital bridge against the same 12 906  $\Omega$  resistance standard employed before, as described in section 3.

The two calibrations are performed at the same operating frequency of 1541.432 697 8 Hz and current of 20  $\mu\text{A}$ . This frequency is chosen to minimize the injections of both the fully-digital bridge and the quadrature bridge. For the fully-digital bridge, the residual deviation from the optimum condition  $W = j$  is about  $3.5 \times 10^{-5}$ .

During the measurement procedure, the 8 nF capacitance standard is kept in a temperature-controlled chamber (Kambic TK-190 US) with a temperature stability better than 4 mK [42]. Since the temperature coefficient of the capacitance standard is  $(4 \pm 6) \times 10^{-6}/^\circ\text{C}$  [43], the maximum effect due to the temperature dependence is about  $4 \times 10^{-8}$  and can be considered virtually negligible with respect to the other uncertainty components. However, even though hermetically sealed in dry nitrogen, the 8 nF capacitance standard shows a significant dependence on the atmospheric pressure [44], evaluated in section 5.1.

### 5.1. Results

The result of the comparison is the relative difference

$$\delta = \frac{C^{\text{fd}} - C^{\text{ref}}}{C^{\text{ref}}}. \quad (20)$$

Figure 5 reports the results of the comparisons performed on 17 and 20 February 2020. Each point in the plot represents the result of the comparison of the average of two successive measurements of  $C^{\text{fd}}$  with one measurement of  $C^{\text{ref}}$ .

For the setup of 17 February, the thresholds were set to 50 nV for the balances at LP1 and LP2 and to 500 nV for the balances at DHP1 and DHP2. For the setup of 20 February, the thresholds were set to 30 nV for the balances at LP1 and LP2 and to 200 nV for the balances at DHP1 and DHP2. The latter set of parameters lead to an improved repeatability and it will be therefore considered an optimal trade-off between repeatability and balancing time.

The dependence on the atmospheric pressure of the 8 nF capacitance standard, introduced in section 5, is checked at regular time intervals with an ultra-precision capacitance bridge (Andeen-Hagerling 2700A). The instability component of the capacitance standard is thus considered for each measurement in the uncertainty of  $\delta$ , which is calculated by combining the uncertainties of  $C^{\text{fd}}$  and  $C^{\text{ref}}$ . The expanded uncertainty of  $C^{\text{ref}}$  is  $U(C^{\text{ref}}) \approx 2 \times 10^{-7}$ , higher than the one stated in [12] to take into account the adaptation of the measuring chain.

In figure 5, the uncertainty bars represent the expanded uncertainties with coverage factor  $k = 2$ .

For the measurements of 20 February, the mean value is  $\delta \approx 3.0 \times 10^{-7}$  with an expanded uncertainty  $U(\delta) \approx 2.9 \times 10^{-7}$ .

## 6. Conclusions and outlook

We presented the design, the implementation and the uncertainty evaluation of a four-terminal-pair fully-digital impedance bridge, optimized for  $RC$  comparisons with 1 : 1 magnitude ratio. Here the bridge was applied to compare a resistance standard with nominal value of  $R_H$  with an 8 nF capacitance standard at 1541 Hz (a 10 nF standard capacitor can be for instance measured at 1233 Hz). We reported the uncertainty budget of an example measurement consisted in 13 repetitions of forward and reverse measurements (overall measurement time of about 200 min). The type A uncertainty component is of  $2.2 \times 10^{-8}$ , while the most significant uncertainty component is that associated to the crosstalk among the channels of the generator, which is about  $8.9 \times 10^{-8}$ . The combined uncertainty is  $9.2 \times 10^{-8}$ , suitable for the primary realization of the unit of

capacitance from a quantized Hall resistance standard. It should be noted that, since the type A uncertainty component is much less than the type B component, 5 measurements (overall measurement time of about 75 min) are enough to reach a combined expanded uncertainty of  $2 \times 10^{-7}$ . The bridge was validated against a suitably modified version of the traceability chain of the Italian national standard of capacitance.

This bridge is intended to be a much simpler, easy-to-operate and affordable alternative to traditional bridges, suitable to be industrially manufactured. Together with the increasing availability of graphene quantum Hall resistance standards, this can provide an affordable quantum realization of the unit farad for metrology institutes and calibration centres. The accuracy can be further improved by means of internal shielding and filtering of the generator to reduce the crosstalk among the channels.

To employ this bridge with a quantized Hall resistance standard it is necessary to adopt a multiple-connection scheme [45] and possibly a double-shield technique [46]. The integration of the bridge with a quantized Hall resistance standard will be the subject of a future work.

## Acknowledgments

This project (18SIB07 GIQS) received funding from the European Metrology Programme for Innovation and Research (EMPIR) co-financed by the Participating States and from the European Unions' Horizon 2020 research and innovation programme.

## References

- [1] Bureau International des Poids et Mesures, "SI brochure, 9th edition," 2019. [Online]. Available: <https://www.bipm.org/utls/common/pdf/si-brochure/SI-Brochure-9-EN.pdf>
- [2] A. Millea and P. Ilie, "A class of double-balance quadrature bridges for the intercomparison of three-terminal resistance, inductance and capacitance standards," *Metrologia*, vol. 5, no. 1, pp. 14–20, 1969.
- [3] L. Callegaro, *Electrical impedance: principles, measurement, and applications*, ser. Series in Sensors. CRC Press, 2013.
- [4] J. C. Hsu and Y.-S. Ku, "Comparison of capacitance with resistance by IVD-based quadrature bridge at frequencies from 50 Hz to 10 kHz," in *Conference on Precision Electromagnetic Measurements (CPEM 2000)*, Sydney, Australia, 14–19 May 2000, pp. 429–430.
- [5] S. Awan, B. Kibble, and J. Schurr, *Coaxial electrical circuits for interference-free measurements*, ser. Electrical Measurement Series. The Institution of Engineering and Technology, 2011.
- [6] S. W. Chua, B. P. Kibble, and A. Hartland, "Comparison of capacitance with ac quantized Hall resistance," *IEEE Trans. Instr. Meas.*, vol. 48, no. 2, pp. 342–345, April 1999.
- [7] G. W. Small, J. R. Fiander, and P. C. Coogan, "A bridge for the comparison of resistance with capacitance at frequencies from 200 Hz to 2 kHz," *Metrologia*, vol. 38, no. 4, pp. 363–368, aug 2001.
- [8] J. Boháček, "A multifrequency quadrature bridge," in *IMTC 2001. Proceedings of the 18th IEEE Instrumentation and Measurement Technology Conference.*, vol. 1, Budapest, Hungary, 21–23 May 2001, pp. 102–105 Vol. 1.
- [9] PTB, NPL, IEN, METAS, CTU, NML, and INETI, "Modular system for the calibration of capacitance standards based on the quantum Hall effect. documentation and operating manual," Eur. Project SMT4-CT98–2231 Final Rep., 2001.
- [10] J. Melcher, J. Schurr, K. Pierz, J. M. Williams, S. P. Giblin, F. Cabiati, L. Callegaro, G. Marullo-Reedtz, C. Cassiago, B. Jeckelmann, B. Jeanneret, F. Overney, J. Bohacek, J. Riha, O. Power, J. Murray, M. Nunes, M. Lobo, and I. Godinho, "The European ACQHE project: modular system for the calibration of capacitance standards based on the quantum Hall effect," *IEEE Trans. Instrum. Meas.*, vol. 52, pp. 563–568, 2003.
- [11] B. Trinchera, L. Callegaro, and V. D'Elia, "Quadrature bridge for  $R$ - $C$  comparisons based on polyphase digital synthesis," *IEEE Trans. Instrum. Meas.*, vol. 58, pp. 202–206, 2009. [Online]. Available: <http://ieeexplore.ieee.org/document/4601488/>
- [12] L. Callegaro, V. D'Elia, and B. Trinchera, "Realization of the farad from the dc quantum Hall effect with digitally assisted impedance bridges," *Metrologia*, vol. 47, pp. 464–472, 2010.
- [13] A. Jeffery, R. E. Elmquist, J. Q. Shields, L. H. Lee, M. E. Cage, S. H. Shields, and R. F. Dziuba, "Determination of the von Klitzing constant and the fine-structure constant through a comparison of the quantized Hall resistance and the ohm derived from the NIST calculable capacitor," *Metrologia*, vol. 35, no. 2, pp. 83–96, apr 1998.
- [14] S. A. Awan, R. G. Jones, and B. P. Kibble, "Evaluation of coaxial bridge systems for accurate determination of the SI farad from the DC quantum hall effect," *Metrologia*, vol. 40, no. 5, pp. 264–270, sep 2003.
- [15] D. L. H. Gibbings, "A design for resistors of calculable a.c./d.c. resistance ratio," *Proc. Inst. Elec. Eng.*, vol. 110, pp. 335–347, 1963.
- [16] R. J. Haddad, "A resistor calculable from DC to  $\omega = 10^5$  rad/s," *Sch. Eng. Appl. Sci.*, George Washington Univ., M. S. Thesis, Apr. 1969.
- [17] J. Schurr, V. Bürkel, and B. P. Kibble, "Realizing the farad from two ac quantum Hall resistances," *Metrologia*, vol. 46, no. 6, p. 619, 2009.
- [18] J. Schurr, F. J. Ahlers, G. Hein, and K. Pierz, "The ac quantum Hall effect as a primary standard of impedance," *Metrologia*, vol. 44, no. 1, pp. 15–23, dec 2006.
- [19] J. Schurr, J. Kučera, K. Pierz, and B. P. Kibble, "The quantum Hall impedance standard," *Metrologia*, vol. 48, no. 1, pp. 47–57, jan 2011.
- [20] H. Bachmair and R. Vollmert, "Comparison of admittances by means of a digital double-sinewave generator," *IEEE Trans. Instrum. Meas.*, vol. 29, pp. 370–372, 1980.
- [21] G. Ramm and H. Moser, "Calibration of electronic capacitance and dissipation factor bridges," *IEEE Trans. Instrum. Meas.*, vol. 52, pp. 396–399, 2003. [Online]. Available: <http://ieeexplore.ieee.org/document/1202056/>
- [22] J. Lan, Z. Zhang, Z. Li, Q. He, J. Zhao, and Z. Lu, "A digital compensation bridge for  $R$ - $C$  comparisons," *Metrologia*, vol. 49, p. 266, 2012. [Online]. Available: <http://stacks.iop.org/0026-1394/49/i=3/a=266>
- [23] L. Callegaro, V. D'Elia, M. Kampik, D. B. Kim, M. Ortolano, and F. Pourdanesh, "Experiences with a two-terminal-pair digital impedance bridge," *IEEE Trans. Instrum. Meas.*, vol. 64, pp. 1460–1465,

2015. [Online]. Available: <http://ieeexplore.ieee.org/document/7051226/>
- [24] W. G. Kürten Ihlenfeld and R. T. de Barros e Vasconcellos, “A digital five-terminal impedance bridge,” *IEEE Trans. Instrum. Meas.*, vol. 66, pp. 1546–1552, 2017. [Online]. Available: <http://ieeexplore.ieee.org/document/7867092/>
- [25] J. Kučera and J. Kováč, “A reconfigurable four terminal-pair digitally assisted and fully digital impedance ratio bridge,” *IEEE Trans. Instrum. Meas.*, vol. 67, pp. 1199–1206, 2018. [Online]. Available: <https://ieeexplore.ieee.org/document/8295009/>
- [26] M. Kruskopf and R. E. Elmquist, “Epitaxial graphene for quantum resistance metrology,” *Metrologia*, vol. 55, no. 4, pp. R27–R36, jul 2018.
- [27] “GIQS — Graphene impedance quantum standard — EMPIR 18SIB07,” Online. [Online]. Available: <https://www.ptb.de/empir2019/giqs/home/>
- [28] F. Overney, N. E. Flowers-Jacobs, B. Jeanneret, A. Rüfenacht, A. E. Fox, J. M. Underwood, A. D. Koffman, and S. P. Benz, “Josephson-based full digital bridge for high-accuracy impedance comparisons,” *Metrologia*, vol. 53, pp. 1045–1053, 2016. [Online]. Available: <http://stacks.iop.org/0026-1394/53/i=4/a=1045>
- [29] S. Bauer, R. Behr, T. Hagen, O. Kieler, J. Lee, L. Palafox, and J. Schurr, “A novel two-terminal-pair pulse-driven Josephson impedance bridge linking a 10 nF capacitance standard to the quantized Hall resistance,” *Metrologia*, vol. 54, pp. 152–160, 2017. [Online]. Available: <http://stacks.iop.org/0026-1394/54/i=2/a=152>
- [30] T. Hagen, L. Palafox, and R. Behr, “A Josephson impedance bridge based on programmable Josephson voltage standards,” *IEEE Trans. Instrum. Meas.*, vol. 66, pp. 1539–1545, 2017. [Online]. Available: <http://ieeexplore.ieee.org/document/7857806/>
- [31] F. Overney, N. E. Flowers-Jacobs, B. Jeanneret, A. Rüfenacht, A. E. Fox, P. D. Dresselhaus, and S. Benz, “Dual Josephson impedance bridge: towards a universal bridge for impedance metrology,” *Metrologia*, 2020, in press.
- [32] P. Gournay, B. Rolland, R. Chayramy, F. Overney, Y. Yang, L. Huang, Z. Lu, Y. Wang, A. Koffman, L. Johnson, R. Xie, J. Belliss, S. Giblin, B. Thornton, J. Schurr, J. Lee, and Y. Semenov, “Comparison CCEM-K4.2017 of 10 pF and 100 pF capacitance standards,” *Metrologia*, vol. 56, no. 1A, pp. 01 001–01 001, nov 2018.
- [33] M. Koziol, J. Kaczmarek, and R. Rybski, “Characterization of PXI-based generators for impedance measurement setups,” in *2018 Conf. Precis. Electromagn. Meas. (CPEM 2018)*. Paris, France: IEEE, 7 2018, pp. 1–2. [Online]. Available: <https://ieeexplore.ieee.org/document/8500928/>
- [34] M. Ortolano, M. Marzano, V. D’Elia, N. T. M. Tran, R. Rybski, J. Kaczmarek, M. Koziol, K. Musiol, A. Christensen, A. Pokatilov, L. Callegaro, J. Kučera, and O. Power, “Error sources in electronic fully-digital impedance bridges,” in *2020 Conf. Precis. Electromagn. Meas. (CPEM 2020)*, 2020, pp. 1–2.
- [35] J. Kaczmarek, R. Rybski, and M. Koziol, “The polyphase ac voltage source for digital impedance bridges,” in *Final dissemination workshop of EMRP projects AIM QuTE, GraphOhm and Q-WAVE*, Prague, 5 2016. [Online]. Available: <https://www.ptb.de/emrp/sib53-finalworkshop.html>
- [36] M. Ortolano, L. Palafox, J. Kučera, L. Callegaro, V. D’Elia, M. Marzano, F. Overney, and G. Gülmez, “An international comparison of phase angle standards between the novel impedance bridges of CMI, INRIM and METAS,” *Metrologia*, vol. 55, pp. 499–512, 2018. [Online]. Available: <http://stacks.iop.org/0026-1394/55/i=4/a=499?key=crossref.c2cd7a61e996537d8e46c442eed3ddaa>
- [37] M. Kampik, J. Torarski, M. M. W. Barwinek, R. Rybski, J. Kaczmarek, and M. K. J. Nissilä, “Comparison of two buffers for impedance metrology,” *Meas. Autom. Monit.*, vol. 61, pp. 127–131, 2015.
- [38] P. Symons, *Digital waveform generation*. Cambridge: Cambridge University Press, 2013.
- [39] L. Callegaro, “On strategies for automatic bridge balancing,” *IEEE Trans. Instrum. Meas.*, vol. 54, pp. 529–532, 2005. [Online]. Available: <http://ieeexplore.ieee.org/document/1408226/>
- [40] “JCGM 102:2011, Evaluation of measurement data — Supplement 2 to the “Guide to the expression of uncertainty in measurement” — Extension to any number of output quantities,” 2011. [Online]. Available: <https://www.bipm.org/en/publications/guides/gum.html>
- [41] M. Zeier, J. Hoffmann, and M. Wollensack, “*Metas.UncLib*—a measurement uncertainty calculator for advanced problems,” *Metrologia*, vol. 49, p. 809, 2012.
- [42] Kambič, *Air bath TK-190 US data sheet*.
- [43] I. Labs, *1404 Series Primary Standard Capacitor Data-sheet*.
- [44] V. D’Elia, L. Callegaro, and M. Ortolano, “Capacitance dependence versus atmospheric pressure of sealed-gas capacitors,” INRIM, TR 23/2018, May 2018.
- [45] F. Delahaye, “Series and parallel connection of multiterminal quantum Hall-effect devices,” *J. Appl. Phys.*, vol. 73, no. 11, pp. 7914–7920, 1993.
- [46] B. P. Kibble and G. H. Rayner, *Coaxial AC bridges*. Bristol, UK: Adam Hilger Ltd, 1984.